

Article

Highly Active Ruthenium Catalyst Supported on Magnetically Separable Mesoporous Organosilica Nanoparticles

Suheir Omar and Raed Abu-Reziq * 

Institute of Chemistry, Casali Center of Applied Chemistry, Center for Nanoscience and Nanotechnology, the Hebrew University of Jerusalem, Jerusalem 9190401, Israel; suheir.omar@mail.huji.ac.il

* Correspondence: Raed.Abu-Reziq@mail.huji.ac.il; Tel.: +972-2-658-6097

Received: 19 July 2020; Accepted: 14 August 2020; Published: 20 August 2020



Abstract: A facile and direct method for synthesizing magnetic periodic mesoporous organosilica nanoparticles from pure organosilane precursors is described. Magnetic ethylene- and phenylene-bridged periodic mesoporous organosilica nanoparticles (PMO NPs) were prepared by nanoemulsification techniques. For fabricating magnetic ethylene- or phenylene-bridged PMO NPs, hydrophobic magnetic nanoparticles in an oil-in-water (o/w) emulsion were prepared, followed by a sol-gel condensation of the incorporated bridged organosilane precursor (1,2 bis(triethoxysilyl)ethane or 1,4 bis(triethoxysilyl)benzene), respectively. The resulting materials were characterized using high-resolution scanning electron microscopy (HR-SEM), high-resolution transmission electron microscopy (HR-TEM), energy-dispersive X-ray (EDX) spectroscopy, powder X-ray diffraction (XRD), solid-state NMR analysis, and nitrogen sorption analysis (N₂-BET). The magnetic ethylene-bridged PMO NPs were successfully loaded using a ruthenium oxide catalyst by means of sonication and evaporation under mild conditions. The obtained catalytic system, termed Ru@M-Ethylene-PMO NPS, was applied in a reduction reaction of aromatic compounds. It exhibited very high catalytic behavior with easy separation from the reaction medium by applying an external magnetic field.

Keywords: periodic mesoporous organosilica nanoparticles; magnetic nanoparticles; ruthenium nanoparticles; catalysis; hydrogenation of aromatic compounds

1. Introduction

Since the discovery of periodic mesoporous organosilica (PMO) bulk materials in 1999 by three independent groups [1–3], they have been studied intensively because of their great potential in designing and fabricating new organic–inorganic hybrid materials with unique properties including high surface areas, high thermal stability, as well as facile separation and recovery as solid materials [4–21]. Recently, much attention has been devoted to developing nanometric-sized PMOs by utilizing organosilane monomers or mixtures of monomers [22–24]. Research on periodic mesoporous organosilica nanoparticles has covered numerous interests including biological [25–27], chemical [28–34], but mostly biomedical applications [35–48]. PMO nanomaterials with special structures and compositions have also been utilized as superior nanosupports for variable metal catalysts [49]. The homogeneous distribution of organic molecules in their frameworks and their uniform mesopores provides them with advantageous properties for hosting metal catalysts or metal nanoparticles within their voids and channels. Because of these features, catalytic transformations mediated by these PMO nanomaterials have been highly studied, developed and utilized [50–53]. However, the ability to recycle these nanoreactors from the reaction medium remains one of the most challenging issues, but which has gained much less attention. The use of magnetic

nanoparticles (MNPs) has offered an attractive and plausible solution for such recovery problems in many fields [54–65]. MNPs have received a great deal of attention because of their low costs, high surface areas, negligible toxicity, and their superparamagnetic properties [66–69]. Owing to their unique properties, magnetic nanoparticles have become highly welcome in many biological [70–75], chemical [76–84], and biomedical domains [85–91]. Lately, very few research groups have reported the preparation of magnetically recoverable PMO nanomaterials for different applications [92–97]. Magnetic periodic mesoporous organosilicas were prepared by utilizing different synthetic routes including the well-known Stöber process [98,99], the microemulsion method [100,101] and a hard template strategy for preparing yolk-shell nanospheres [94,97]. All these systems were mostly prepared from a mixture of an organosilane monomer and tetraorthosilicate and were applied in different catalytic transformations. Herein, we describe the synthesis of magnetic ethylene- and phenylene-bridged PMO NPs that were prepared by a sol–gel process under mild conditions from pure organosilane precursors in the presence of a cetyltrimethylammonium bromide (CTAB) surfactant with the addition of hydrophobic magnetite nanoparticles. Both magnetic ethylene- and phenylene-bridged PMO NPs were successfully obtained; however, they displayed different morphological and textural properties. The magnetic ethylene-bridged PMO NPs (M-Ethylene-PMO NPs) exhibited highly ordered mesostructures, whereas magnetic phenylene-bridged PMO NPs (M-Phenylene-PMO NPs) exhibited smooth surface nanoparticles with no specific mesostructure ordering. M-Ethylene-PMO NPs were loaded with ruthenium oxide nanoparticles by means of sonication and evaporation under mild conditions and the resulting catalytic magnetic PMO nanoreactors, termed Ru@M-Ethylene PMO NPs, were utilized in the reduction reaction of aromatic compounds because they exhibited excellent catalytic behavior.

2. Materials and Methods

2.1. General Information

X-ray powder diffraction (XRD) patterns were measured using a D8 advanced diffractometer (Bruker AXS, Karlsruhe, Germany) with $\text{CuK}\alpha$ radiation. A PerkinElmer (FTIR 65) spectrometer was utilized to record the infrared spectra. Scanning electron microscopy (SEM) was carried out using a Sirion SEM microscope (FEI Company, Hillsboro, OR, USA), a Shottky-type emission source, and a secondary electron (SE) detector, operated at a voltage of 5 kV. Transmission electron microscopy (TEM), scanning transmission electron microscopy (STEM), and electron diffraction spectroscopy (EDS) analyses were accomplished through (S)TEM Tecnai F20 G2 (FEI Company, Hillsboro, OR, USA) operated at 200 kV. Size distribution and zeta potential were determined by a Nano Series instrument, model Nano-Zetasizer ZEN3600 (Malvern Instruments, Worcestershire, United Kingdom). Thermogravimetric analysis (TGA) was done on a Mettler Toledo TG 50 analyzer (Greifensee, Switzerland). Measurements were conducted at a temperature range from 25 to 900 °C at a heating rate of 10 °C/min under an inert atmosphere (N_2). The specific surface areas were calculated by means of the Brunauer–Emmett–Teller (BET) equation by utilizing a high-speed gas sorption analyzer, and a Quantachrome Nova 1200e instrument (Quantachrome Instruments, Boynton Beach, USA). The reaction mixtures were analyzed by gas chromatography (GC) (Agilent Technologies, 7890A, Santa Clara, USA) with a universal capillary column (HP-5, 30 m) to determine the yields and the conversions of the reactions. ^1H NMR and ^{13}C NMR spectra were recorded using a Bruker DRX-400 and DRX-500 instrument (Rheinstetten, Germany). Inductively coupled plasma mass spectrometry measurements (ICP) were done on a 7500cx instrument (Agilent company, Tokyo, Japan) using an external standard calibration to determine the ruthenium loadings.

2.2. Materials

1,2 Bis(triethoxysilyl)ethane, 1,4 Bis(triethoxysilyl)benzene, cetyltrimethylammonium bromide (CTAB), ammonium hydroxide (25% aqueous solution), oleic acid, iron dichloride tetrahydrate,

and iron trichloride hexahydrate were obtained from Sigma–Aldrich. All chemicals were used without further purification.

2.3. Synthesis of Hydrophobic Magnetite Nanoparticles Functionalized with Oleic Acid (MNP-OA)

The magnetite nanoparticles were prepared following the Massart procedure: [102] Briefly, $\text{FeCl}_3 \cdot 6\text{H}_2\text{O}$ (11.7 g) and 4.23 g of $\text{FeCl}_2 \cdot 4\text{H}_2\text{O}$ were dissolved in 400 mL of distilled water under N_2 with vigorous mechanical stirring at 90 °C. Then, 18 mL of NH_4OH (25%) were quickly added to the solution and the resulting mixture was stirred at the same temperature for additional 20 min. After that, 18 mL of oleic acid was added dropwise to the reaction mixture and stirring continued at 90 °C for a further 1 h. After cooling to room temperature, a black precipitate was collected by magnetic decantation and washed several times with water and acetone. The resulting magnetite nanoparticles were dispersed in 100 mL of chloroform. This dispersion was sonicated for 60 min before its use.

2.4. Synthesis of the Magnetic PMO Nanoparticles (Magnetic PMO NPs)

The preparation of magnetic ethylene- and phenylene-bridged PMO nanoparticles was based on the following steps: CTAB (0.48 g), distilled water (88 mL), ethanol (33 mL), and 25% aqueous ammonia (0.1 mL) were mixed. Then, the bridged organosilane monomer (3.5 mmol) and 1 mL of hydrophobic magnetite (MNP-OA) were dropped into the mixture under stirring. The mixture was mechanically stirred for 24 h at room temperature. The solid product was then collected using an external magnet and the CTAB surfactant was extracted ethanol for 24 h using soxhlet extractor. The final magnetic PMO NPs were dried at 54 °C for 16 h to afford a fine black-brownish powder for both systems.

2.5. Supporting Ruthenium Oxide Nanoparticles on the Magnetic Ethylene-PMO NPs

One hundred mg of solid magnetic ethylene-PMO NPs and 7 mg of $\text{RuO}_2 \cdot x\text{H}_2\text{O}$ catalyst (0.05 mmol) were dispersed in 30 mL of methanol, and after sonication for 1 h the resulting mixture was stirred for 24 h at room temperature. Then, the solvent was evaporated under reduced pressure and the solid catalytic Ru@M-Ethylene PMO NP material was washed three times with methanol and dried at 54 °C for 16 h. The ruthenium loading of Ru@M-Ethylene PMO NPs was 0.43 mmol g^{-1} , as was determined by inductively coupled plasma mass spectrometry (ICP) analysis.

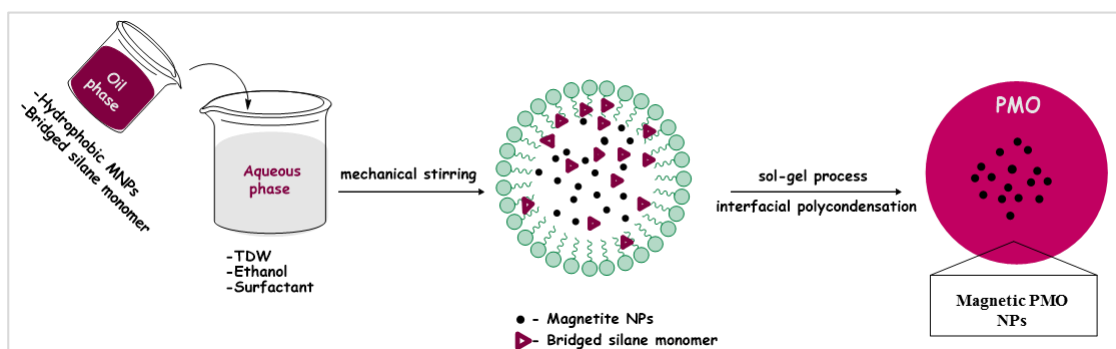
2.6. General Procedure for the Hydrogenation of Aromatic Compounds Mediated by Ru@M-Ethylene PMO NPs

A mixture of 1 mmol substrate and 2.5 mg of Ru@M-Ethylene PMO NP catalyst (0.001 mmol Ru) in 2 mL heptane was added to a 25 mL glass-lined autoclave vessel. The autoclave was sealed, purged three times with hydrogen, and pressurized to 100–400 psi with hydrogen. The autoclave was heated at 80–120 °C for up to 12 h. After cooling to room temperature, the hydrogen gas was carefully released and the catalyst was isolated from the mixture using external magnet. The products were analyzed by GC and ^1H NMR.

3. Results and Discussion

3.1. Preparation of Catalytic Periodic Mesoporous Organosilica Nanoparticles with Ruthenium Metal Nanoparticles

Magnetic periodic mesoporous organosilica nanoparticles were synthesized in a sol–gel process under mild conditions. At first, the hydrophobic magnetite nanoparticles, together with the silane monomer, were added to the aqueous phase, which included water, ethanol, ammonia catalyst, and a CTAB surfactant to form an oil-in-water microemulsion system. The organosilane begins to hydrolyze and condense under these basic conditions to form magnetic PMO NP systems composed of 100% organo-alkoxysilane precursors in a typical sol–gel process, as illustrated in Scheme 1.



Scheme 1. Illustration of the preparation of magnetic periodic mesoporous organosilica (PMO) nanoparticles.

3.2. Characterization of Magnetic PMO Nanoparticle Systems

The magnetic ethylene- and phenylene-bridged PMO NPs were prepared under similar reaction conditions by utilizing different organosilane monomers. Figure 1a shows a representative scanning electron microscopy (SEM) image in which spherical and monodispersed nanoparticles can be clearly seen. Figure 1b–d, showing TEM images, confirms the presence of magnetic nanoparticles in the cores inside highly ordered mesostructures. It presents scanning transmission electron microscopy (STEM) and transmission electron microscopy (TEM) images of the resulting magnetic ethylene-bridged PMO NPs. Figure 2 shows magnetic phenylene-bridged PMO NPs. Under the same synthetic conditions, the resulting M-Phenylene PMO NPs exhibited different structural and textural properties. The obtained smoothed-surface spherical system exhibited some polydispersity where mesostructure ordering was not clearly observed. However, the magnetite nanoparticles were also settled in the cores of these nanoparticles.

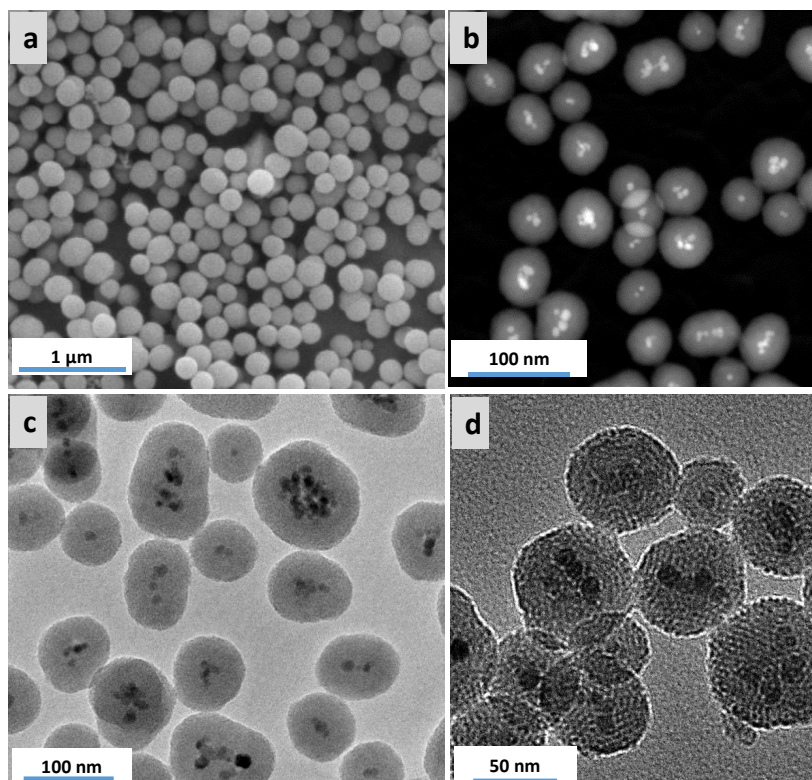


Figure 1. (a) SEM, (b) STEM, and (c–d) TEM micrographs of M-Ethylene PMO NPs.

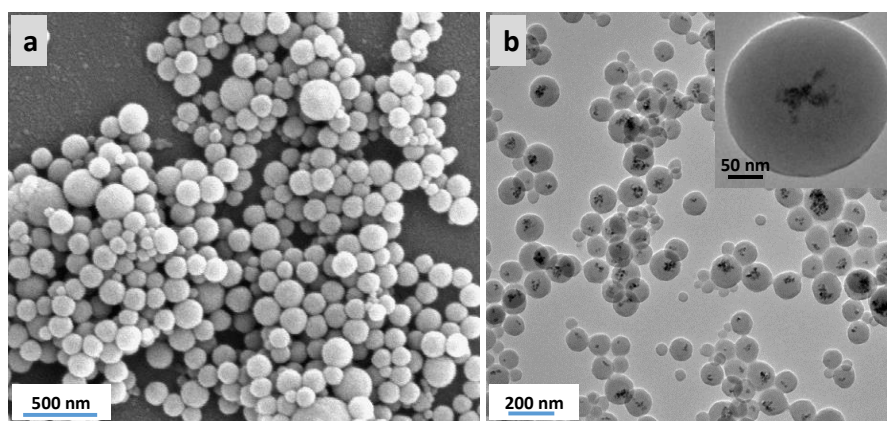


Figure 2. (a) SEM and (b) TEM micrographs of M-Phenylene PMO nanoparticles (NPs).

The average diameter and the outer surface charge of the magnetic PMO nanoparticles were determined by dynamic light scattering analysis (DLS). The obtained average size of M-Ethylene PMO NPs ranged between 85 and 150 nm and their zeta potential value was -28.6 mV (Figure 3). With M-Phenylene PMO NPs, this system exhibited an average diameter of 221.2 nm with a -9.06 mV zeta potential value (Figure 4).

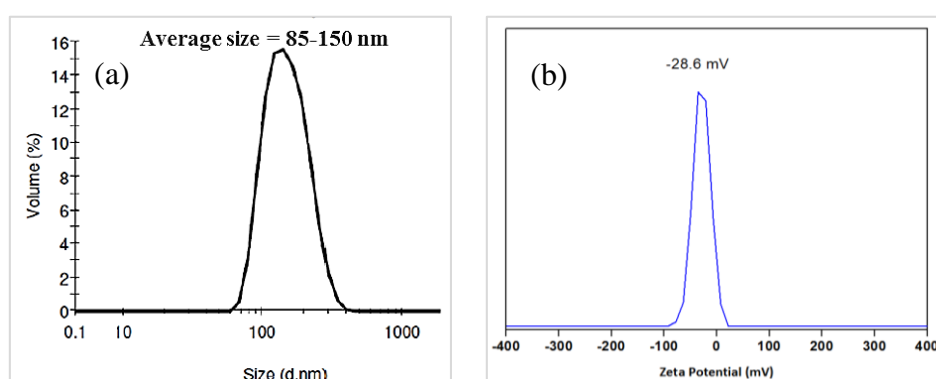


Figure 3. Size distribution (a) and zeta potential analysis (b) of Magnetic Ethylene-PMO NPs.

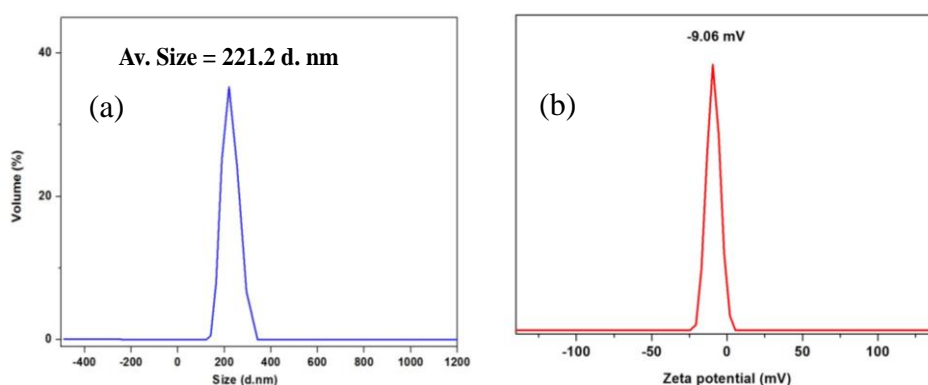


Figure 4. Size distribution (a) and zeta potential (b) analysis of Magnetic Phenylene-PMO NPs.

The obtained magnetic PMO NP systems were further examined using EDX spectroscopy and EDX mapping analysis in order to confirm all the elemental compositions in both systems. From the EDX spectroscopy results shown in Figures 5 and 6, the existence of magnetite nanoparticles inside the

cores was confirmed. As supportive results, the EDX mapping analysis clearly shows the deposition of all other elements including silica and oxygen that compose the particles' silica network, whereas the magnetic nanoparticles were mostly localized in the cores.

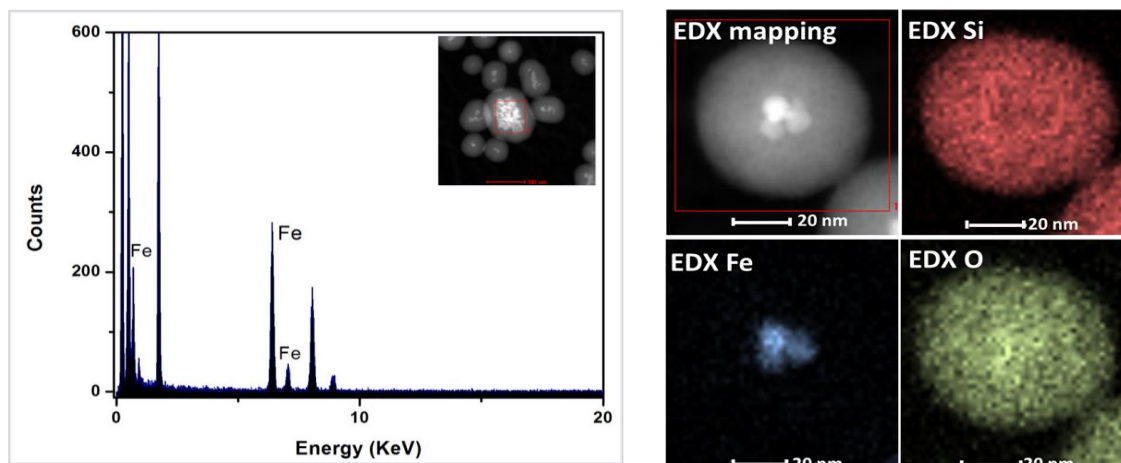


Figure 5. EDX spectroscopy (Left) and EDX mapping analysis (Right) of M-Ethylene PMO NPs.

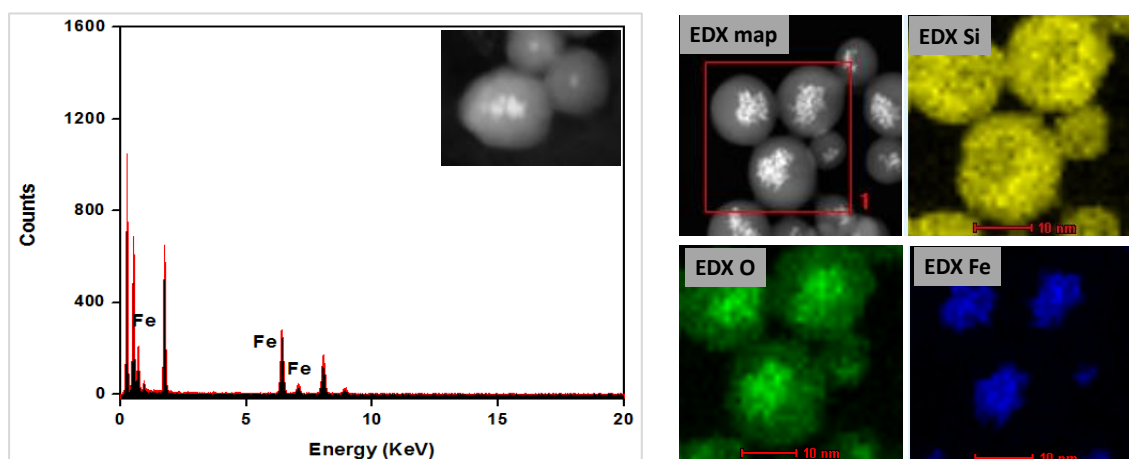


Figure 6. EDX spectroscopy (Left) and EDX mapping analysis (Right) of M-Phenylene PMO NPs.

In addition to the TEM results shown previously, the XRD pattern of M-Ethylene PMO NPs (Figure 7a) indicated a well-resolved peak in the range of $2\theta = 1.5^\circ\text{--}2.5^\circ$, whereas the Phenylene-PNO NPs exhibited a broad XRD peak (Figure 7b), which confirmed the previous TEM results of distorted mesostructures in these nanoparticles. In addition, both XRD patterns exhibited the characteristic peaks of magnetite nanoparticles at $2\theta = 30^\circ, 35^\circ, 43^\circ, 53^\circ, 57^\circ,$ and 63° .

The compositional information of M-Ethylene PMO NPs and M-Phenylene PMO NPs was characterized by FT-IR spectroscopy (Figure 8). The FTIR spectra of both systems were very similar, displaying distinct absorbance peaks at $796, 1028, 1093,$ and 1271 cm^{-1} , which can be assigned to Si-C vibrations. In addition, the absorption bands at 1154 cm^{-1} and at the interval of $2950\text{--}3730\text{ cm}^{-1}$ in both curves are assigned to the asymmetrical stretching of siloxane groups (Si-O-Si) and Si-OH stretching vibrations, respectively. The absorbance peaks at $2850\text{--}2927\text{ cm}^{-1}$ are assigned to C-H stretching from both nanoparticle systems. In addition, the presence of the oleate group coating on the magnetite nanoparticles is indicated by the bands at the interval $2853\text{--}2930$ and 1634 cm^{-1} , which are attributed to the stretching of C-H and the C=C groups, respectively.

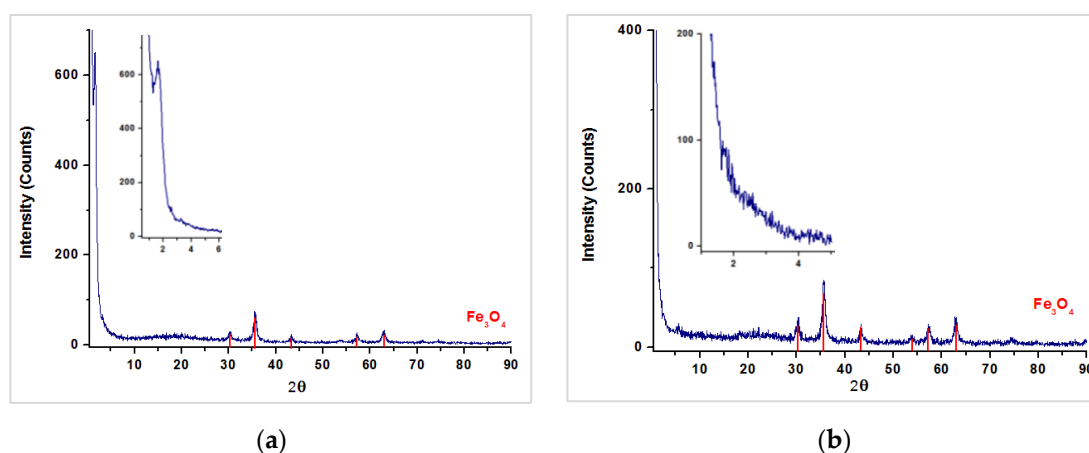


Figure 7. XRD pattern of (a) M-Ethylene PMO NPs and (b) M-Phenylene PMO NPs.

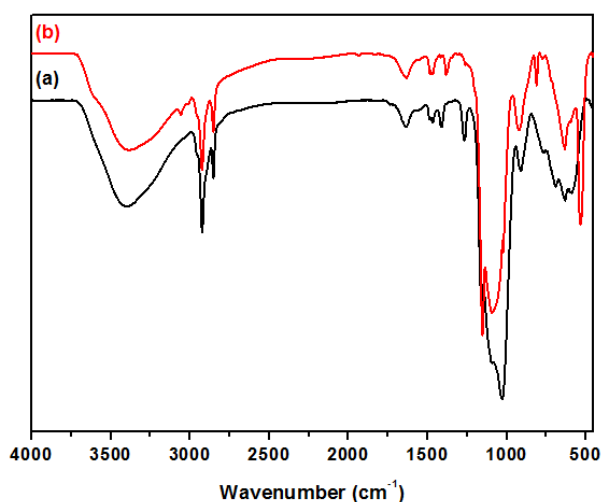


Figure 8. IR spectra of (a) M-Ethylene PMO NPs and (b) M-Phenylene PMO NPs.

The organic contents of the magnetic PMO nanoparticles were tested by thermogravimetric analysis (TGA). In both systems, slight decomposition occurred in the temperature range of 50–100 °C, which could have resulted from ethanol and water residues in the detected system, whereas a major decomposition process occurred between 200 and 650 °C. This confirms the good thermal stability of the synthesized magnetic PMO nanoparticles compared with the oleic acid-coated MNPs. Figure 9 shows curve a, in which a total weight loss of 13.47% was detected for MNP-OA, whereas M-Ethylene PMO NPs afforded a total organic loss of 23.7% (Figure 9, curve b) compared to 37.4% for M-Phenylene PMO NPs (Figure 9, curve c).

The PMO NPs' chemical properties were further characterized by solid-state ^{29}Si and ^{13}C CP-MAS NMR spectroscopy. The solid-state NMR results of these magnetic systems were recorded after treatment with concentrated HCl to remove the magnetic cores. The ^{29}Si NMR spectrum of M-Ethylene PMO NPs (Figure 10a) exhibits a major T^3 signal at -65 ppm, which can be assigned to organosilica species. Similar results were observed in the ^{29}Si NMR spectrum of M-Phenylene PMO NPs (Figure 10c), which exhibited three T signals at -58 , -71 , and -80 ppm. The observed signals are assigned to the T^2 and T^3 groups in the resulting organosilica network. These observations clearly demonstrate the formation of Si-C covalent bonds in both magnetic PMO NP systems. In addition, the ^{13}C NMR spectrum of the M-Ethylene PMO NPs in Figure 10b shows the chemical composition of the ethylene-bridged nanoparticles with a major peak around 8–10 ppm, which belongs to the SiCH_2

groups. Two minor peaks of unhydrolyzed ethoxy groups at 13 ppm and 56 were also observed in the ^{13}C NMR spectrum. In Figure 10d, the ^{13}C NMR spectrum of M-Phenylene PMO NPs also confirms the presence of the aromatic c groups that clearly appear at a range of 128–147 ppm. In addition, in this spectrum, unhydrolyzed ethoxy groups were detected. These results clearly indicate the formation of silsesquioxane frameworks and further demonstrate the incorporation of organic units into the silica networks.

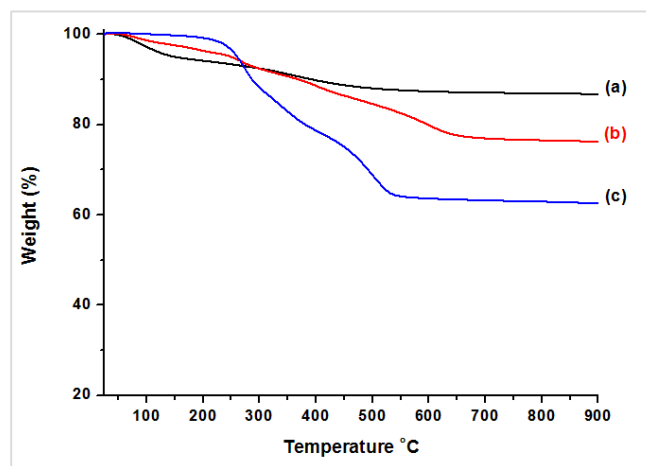


Figure 9. Thermogravimetric analysis (TGA) curves of (a) MNP-OA, (b) Magnetic Ethylene-PMO NPs, and (c) Magnetic Phenylene-PMO NPs.

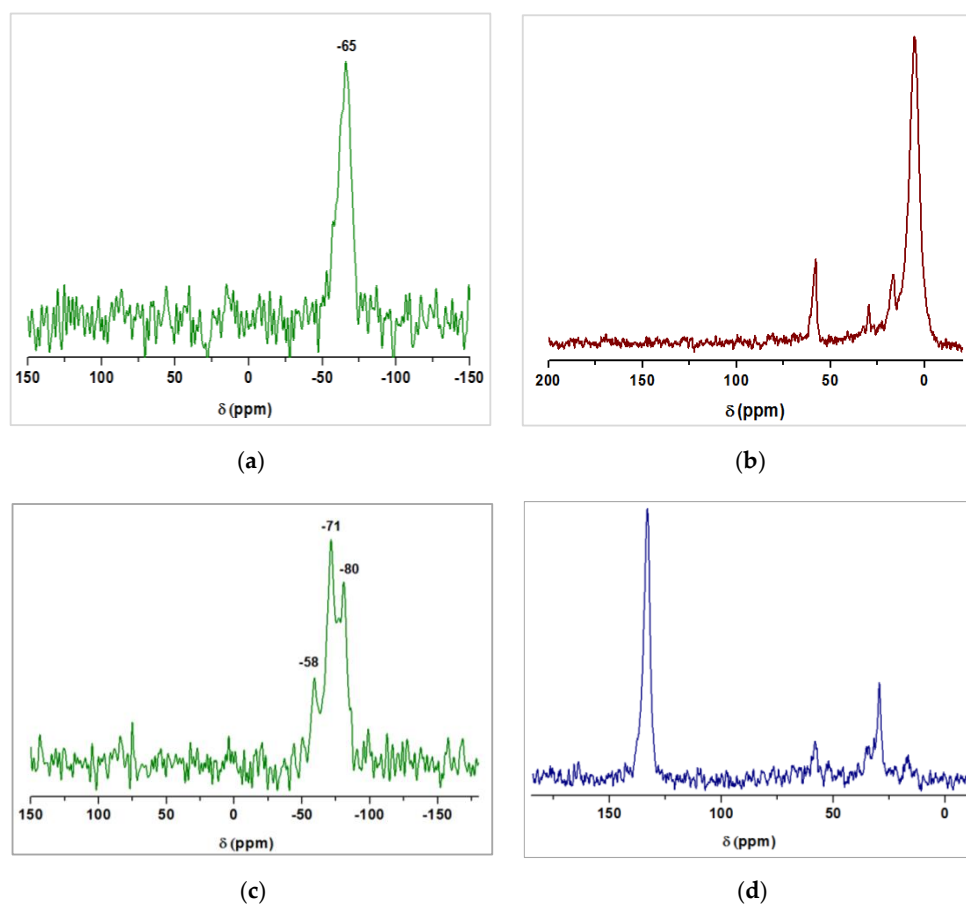


Figure 10. ^{29}Si and ^{13}C CP-MAS of M-Ethylene PMO-NPs (a,b) and M-Phenylene PMO NPs (c,d).

The N_2 adsorption-desorption of M-Ethylene PMO NPs and M-Phenylene PMO NPs provides further evidence of the special porosity character of the obtained magnetic nanosystems. As observed in Figure 11, characteristic IV-type isotherms with a narrow pore size distribution for both magnetic PMO nanoparticles were obtained. The BET surface area of Magnetic Ethylene-PMO NPs was calculated to be $743 \text{ m}^2/\text{g}$ with a pore radius of 2.47 nm. It was calculated by the Barrett–Joyner–Halenda (BJH) method, whereas the surface area of Phenylene-PMO NPs was calculated to be $611 \text{ m}^2/\text{g}$ with a pore radius of 1.54 nm, according to BJH calculations. It is worth mentioning that incorporating the magnetic nanoparticles into the cores did not dramatically affect the total surface area value of the synthesized systems.

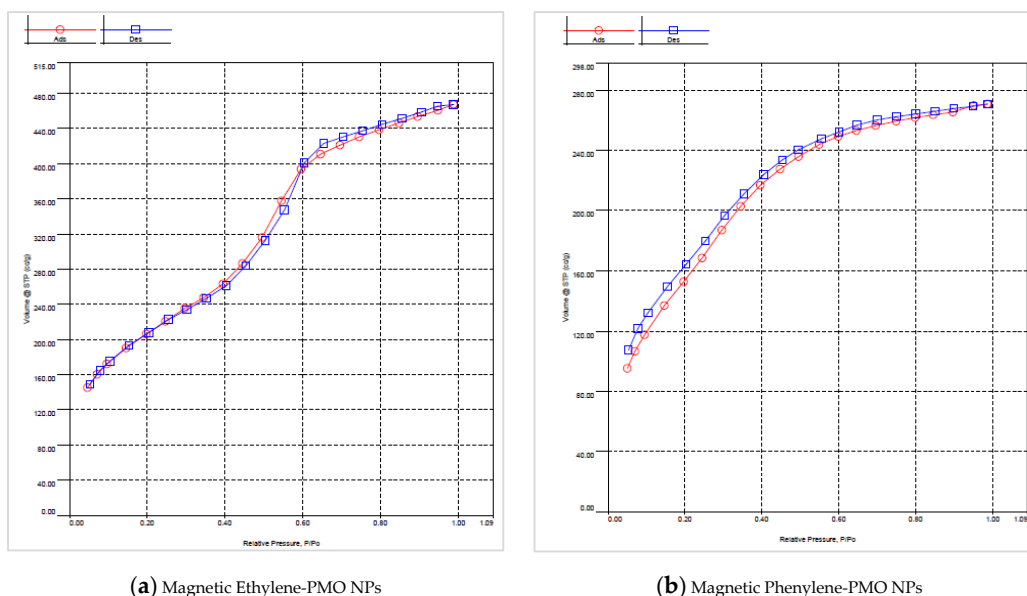
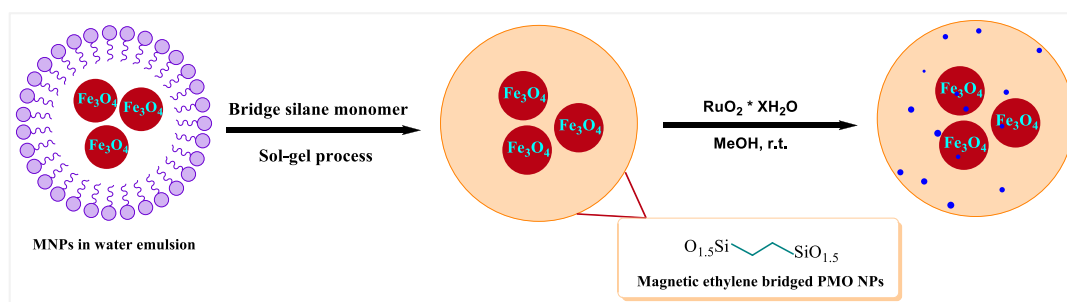


Figure 11. N_2 adsorption-desorption isotherms of (a) M-Ethylene PMO NPs and (b) M-Phenylene PMO NPs.

3.3. Preparation and Characterization of Magnetic Ethylene-PMO NP Catalytic Systems

After their structural and chemical properties were examined, the magnetic ethylene-bridged PMO NPs were loaded with ruthenium oxide nanoparticles by means of sonication and evaporation under mild conditions to afford catalytic $\text{Ru}@$ M-Ethylene PMO NPs, as depicted in Scheme 2. From the STEM-EDX mapping results in Figure 12, it can be concluded that the ruthenium oxide was successfully immobilized.



Scheme 2. Preparation of the $\text{Ru}@$ M-Ethylene PMO NP catalytic system.

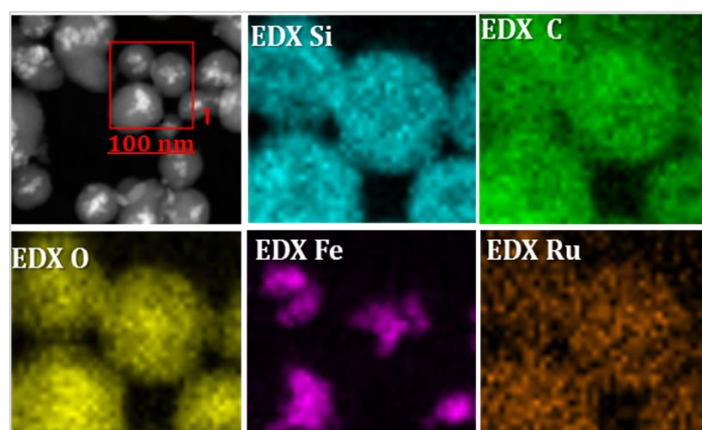


Figure 12. STEM-EDX mapping analysis of Ru@M-Ethylene PMO NPs.

The EDX-mapping analysis confirms the presence of ruthenium nanoparticles because they were homogeneously distributed at a lower density (orange map) compared with all other elements including silicon, carbon, and oxygen, which were deposited throughout the organosilica framework except for the magnetic nanoparticles, which were observed in a high density only in the cores of the detected Ru@M-Ethylene PMO NP system. In addition, the analysis ruthenium oxide supported on ethylene-PMO nanoparticles by XRD confirmed the formation of ruthenium oxide nanoparticles with crystallite size of 3.54 nm as was calculated by the Scherrer equation (Figure S1, Supporting Information).

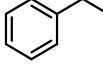
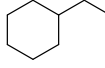
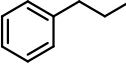
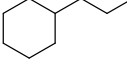
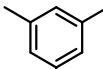
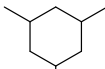
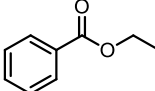
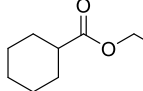
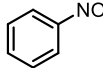
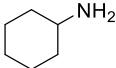
3.4. Catalysis

Ruthenium nanoparticles have widely been used in hydrogenation processes [103–108]. The catalytic activity of Ru@M-Ethylene PMO NPs was examined in a hydrogenation reaction of aromatic compounds as a model reaction. The reduction reaction was performed in heptane solvent at temperatures of 80–120 °C under hydrogen pressures of 100–400 psi with 0.1 mol% of the ruthenium catalyst. From the results presented in Table 1, it can be concluded that the catalyst's efficacy and activity were very high in catalyzing this hydrogenation reaction. Thus, benzene and toluene were fully hydrogenated in one hour and gave cyclohexane and methylcyclohexane, respectively (Table 1, entries 1 and 2, respectively). The hydrogenation of ethylbenzene and propylbenzene required a longer time and a higher temperature to provide the fully hydrogenated products in excellent yields (Table 1, entries 3 and 4, respectively). The substrates *m*-xylene and 1,3,5-trimethylbenzene could be converted after 12 h at 120 °C into a mixture of isomers of alkylated cyclohexanes (Table 1, entries 5 and 6). The catalyst exhibited good reactivity in the hydrogenation of aromatic compounds substituted with electron withdrawing groups. For example, the hydrogenation of ethyl benzoate under 400 psi H₂ and at 120 °C gave ethyl cyclohexanecarboxylate after 12 h in complete conversion. When nitrobenzene was hydrogenated under the same conditions, cyclohexylamine was produced in quantitative yields.

To demonstrate our novel catalytic system activity, further kinetic tests on toluene were performed. From the high turnover number (TON) and turnover frequency (TOF) values displayed in Table 2, it can be concluded that the high catalytic activity of the catalyst is preserved at very high substrate concentrations under the same reaction conditions of 400 psi of hydrogen and a temperature of 80 °C.

In addition, the recyclability of the catalyst was tested in the hydrogenation of toluene with substrate: catalyst ratio of 2000:1 under 400 psi H₂ at 80 °C. The catalyst was reused four times in this reaction without any loss of its reactivity. Inductively coupled plasma mass spectrometry (ICP-MS) analysis indicated that there was no leaching of the ruthenium catalyst during the hydrogenation reaction.

Table 1. Reduction of aromatic compounds mediated by the Ru@M-Ethylene PMO NP catalyst. [a].

Entry	Substrate	H ₂ Pressure	Reaction Time (h)	Temperature	Products	Yield (%) [b]
1		100 psi	1	80 °C		>99
2		100 psi	1	80 °C		>99
3		400 psi	2	120 °C		>99
4		400 psi	4	120 °C		>99
5c		400 psi	12	120 °C		>99
6c		400 psi	12	120 °C		>99
7		400 psi	12	120 °C		>99
8		400 psi	12	120 °C		>99

[a] Reaction conditions: 0.1 mol% catalyst, 2 mL heptane, 1–12 h, 100–400 psi of H₂; [b] determined by ¹H-NMR and GC using hexadecane as internal standard; [c] the product contains mixture of isomers.

Table 2. Reduction of toluene mediated by the Ru@M-Ethylene PMO NP catalyst. [a].

Entry	Substrate	S/C Ratio	Reaction Time (h)	Conversion (%) [b]	TON	TOF (h ⁻¹)
1		1000	0.5	99.6	996	1992
2		2000	1	100	2000	2000
3		5000	1	99.8	4992	4992
4		10,000	1	97.2	9783	9783
5		50,000	1	9.5	4750	4750
6		100,000	1	2	2000	2000

[a] Reaction conditions: 2 mL heptane, 400 psi of H₂; 80 °C; [b] Determined by ¹H-NMR and GC.

4. Conclusions

We succeeded in synthesizing and characterizing new magnetic PMO nanoparticles from pure organosilica precursors. These novel systems were utilized for designing new catalytic nanoreactors

by supporting metal nanoparticles in their mesoscopic channels. The resulting magnetic PMO NPs were loaded with ruthenium oxide nanoparticles without the need for any stabilizing agent. The new magnetic catalytic system was applied in the hydrogenation reaction of aromatic compounds and it exhibited a high catalytic performance. Introducing the magnetic nanoparticles in these nanosystems greatly improves the catalyst's separation and recovery from the reaction medium and eliminates the cumbersome workup and filtering processes. We believe that this successful strategy for designing pure magnetic PMO nanomaterials can provide new opportunities in many catalytic and other scientific areas.

Supplementary Materials: The following are available online at <http://www.mdpi.com/2076-3417/10/17/5769/s1>, Figure S1: XRD pattern of Ru@Ethylene PMO NPs, GC chromatographs and ¹HNMR spectra of the hydrogenation products.

Author Contributions: Conceptualization, R.A.-R.; methodology, R.A.-R. and S.O.; formal analysis, R.A.-R. and S.O.; investigation, S.O.; resources, R.A.-R.; data curation, S.O.; writing—original draft preparation, S.O.; writing—review and editing, R.A.-R. and S.O.; visualization, S.O.; supervision R.A.-R.; project administration, R.A.-R.; funding acquisition, R.A.-R. All authors have read and agreed to the published version of the manuscript.

Funding: This research was funded by Casali Foundation.

Acknowledgments: S. Omar is grateful to the Ministry of Science and Technology of Israel for her fellowship.

Conflicts of Interest: The authors declare no conflict of interest. The funders had no role in the design of the study; in the collection, analyses, or interpretation of data; in the writing of the manuscript, or in the decision to publish the results.

References

1. Melde, B.J.; Holland, B.T.; Blanford, C.F.; Stein, A. Mesoporous sieves with unified hybrid inorganic/organic frameworks. *Chem. Mater.* **1999**, *11*, 3302–3308. [[CrossRef](#)]
2. Inagaki, S.; Guan, S.; Fukushima, Y.; Ohsuna, T.; Terasaki, O. Novel mesoporous materials with a uniform distribution of organic groups and inorganic oxide in their frameworks. *J. Am. Chem. Soc.* **1999**, *121*, 9611–9614. [[CrossRef](#)]
3. Asefa, T.; MacLachlan, M.J.; Coombs, N.; Ozin, G.A. Periodic mesoporous organosilicas with organic groups inside the channel walls. *Nature* **1999**, *402*, 867–871. [[CrossRef](#)]
4. Boury, B.; Corriu, R.J.P. Adjusting the porosity of a silica-based hybrid material. *Adv. Mater.* **2000**, *12*, 989–992. [[CrossRef](#)]
5. Shea, K.J.; Loy, D.A. Bridged polysilsesquioxanes. Molecular-engineered hybrid organic–inorganic materials. *Chem. Mater.* **2001**, *13*, 3306–3319. [[CrossRef](#)]
6. Hunks, W.J.; Ozin, G.A. Challenges and advances in the chemistry of periodic mesoporous organosilicas (PMOs). *J. Mater. Chem.* **2005**, *15*, 3716–3724. [[CrossRef](#)]
7. Vercaemst, C.; De Jongh, P.E.; Meeldijk, J.D.; Goderis, B.; Verpoort, F.; Van Der Voort, P. Ethylene-bridged periodic mesoporous organosilicas with ultra-large mesopores. *Chem. Commun.* **2009**, 4052. [[CrossRef](#)] [[PubMed](#)]
8. Mandal, M.; Manchanda, A.S.; Zhuang, J.; Kruk, M. Face-centered-cubic large-pore periodic mesoporous organosilicas with unsaturated and aromatic bridging groups. *Langmuir* **2012**, *28*, 8737–8745. [[CrossRef](#)] [[PubMed](#)]
9. Rao, K.V.; Jain, A.; George, S.J. Organic–inorganic light-harvesting scaffolds for luminescent hybrids. *J. Mater. Chem. C* **2014**, *2*, 3055–3064. [[CrossRef](#)]
10. Hatton, B.; Landskron, K.; Whitnall, W.; Perovic, D.; Ozin, G.A. Past, present, and future of periodic mesoporous organosilicas the PMOs. *Accounts Chem. Res.* **2005**, *38*, 305–312. [[CrossRef](#)]
11. Waki, M.; Mizoshita, N.; Tani, T.; Inagaki, S. Periodic mesoporous organosilica derivatives bearing a high density of metal complexes on pore surfaces. *Angew. Chem.* **2011**, *123*, 11871–11875. [[CrossRef](#)]
12. Matos, J.R.; Kruk, M.; Mercuri, L.P.; Jaroniec, M.; Asefa, T.; Coombs, N.; Ozin, G.A.; Kamiyama, T.; Terasaki, O. Periodic mesoporous organosilica with large cage-like pores. *Chem. Mater.* **2002**, *14*, 1903–1905. [[CrossRef](#)]
13. Park, S.S.; Moorthy, M.S.; Ha, C.S. Periodic mesoporous organosilicas for advanced applications. *NPG Asia Mater.* **2014**, *6*, e96. [[CrossRef](#)]

14. Van Der Voort, P.; Esquivel, D.; De Canck, E.; Goethals, F.; Van Driessche, I.; Romero-Salguero, F.J. Periodic Mesoporous Organosilicas: From simple to complex bridges; a comprehensive overview of functions, morphologies and applications. *Chem. Soc. Rev.* **2013**, *42*, 3913–3955. [[CrossRef](#)] [[PubMed](#)]
15. Wahab, M.A.; Beltramini, J.N. Recent advances in hybrid periodic mesostructured organosilica materials: Opportunities from fundamental to biomedical applications. *RSC Adv.* **2015**, *5*, 79129–79151. [[CrossRef](#)]
16. Descalzo, A.B.; Martínez-Mañez, R.; Sancenón, F.; Hoffmann, K.; Rurack, K. The supramolecular chemistry of organic–inorganic hybrid materials. *Angew. Chem. Int. Ed.* **2006**, *45*, 5924–5948. [[CrossRef](#)]
17. Mizoshita, N.; Tani, T.; Inagaki, S. Syntheses, properties and applications of periodic mesoporous organosilicas prepared from bridged organosilane precursors. *Chem. Soc. Rev.* **2011**, *40*, 789–800. [[CrossRef](#)]
18. Morell, J.; Wolter, G.; Fröba, M. Synthesis and characterization of highly ordered thiophene-bridged periodic mesoporous organosilicas with large pores. *Chem. Mater.* **2005**, *17*, 804–808. [[CrossRef](#)]
19. Xia, H.S.; Zhou, C.H. (Clayton); Tong, D.S.; Lin, C.X. Synthesis chemistry and application development of periodic mesoporous organosilicas. *J. Porous Mater.* **2009**, *17*, 225–252. [[CrossRef](#)]
20. Wang, W.; Lofgreen, J.E.; Ozin, G.A. Why PMO? Towards functionality and utility of periodic mesoporous organosilicas. *Small* **2010**, *6*, 2634–2642. [[CrossRef](#)]
21. Auras, F.; Li, Y.; Löbermann, F.; Döblinger, M.; Schuster, J.; Peter, L.M.; Trauner, D.; Bein, T. A Zinc Phthalocyanine based periodic mesoporous organosilica exhibiting charge transfer to fullerenes. *Chem. Eur. J.* **2014**, *20*, 14971–14975. [[CrossRef](#)] [[PubMed](#)]
22. Guan, B.; Cui, Y.; Ren, Z.; Qiao, Z.-A.; Wang, L.; Liu, Y.; Huo, Q. Highly ordered periodic mesoporous organosilica nanoparticles with controllable pore structures. *Nanoscale* **2012**, *4*, 6588–6596. [[CrossRef](#)] [[PubMed](#)]
23. Djojoputro, H.; Zhou, X.F.; Qiao, S.; Wang, L.; Yu, C.; Lu, G. Periodic mesoporous organosilica hollow spheres with tunable wall thickness. *J. Am. Chem. Soc.* **2006**, *128*, 6320–6321. [[CrossRef](#)] [[PubMed](#)]
24. Croissant, J.G.; Cattoen, X.; Man, M.W.C.; Durand, J.O.; Khashab, N.M. Syntheses and applications of periodic mesoporous organosilica nanoparticles. *Nanoscale* **2015**, *7*, 20318–20334. [[CrossRef](#)] [[PubMed](#)]
25. Chen, Y.; Shi, J.L. Chemistry of mesoporous organosilica in nanotechnology: Molecularly organic-inorganic hybridization into frameworks. *Adv. Mater.* **2016**, *28*, 3235–3272. [[CrossRef](#)]
26. Gao, J.; Zhang, X.; Xu, S.; Tan, F.; Li, X.; Zhang, Y.; Qu, Z.; Quan, X.; Liu, J. Clickable periodic mesoporous organosilicas: Synthesis, click reactions, and adsorption of antibiotics. *Chem. Eur. J.* **2013**, *20*, 1957–1963. [[CrossRef](#)] [[PubMed](#)]
27. Yamamoto, Y.; Takeda, H.; Yui, T.; Ueda, Y.; Koike, K.; Inagaki, S.; Ishitani, O. Efficient light harvesting via sequential two-step energy accumulation using a Ru–Re5 multinuclear complex incorporated into periodic mesoporous organosilica. *Chem. Sci.* **2014**, *5*, 639–648. [[CrossRef](#)]
28. Ide, M.; De Canck, E.; Van Driessche, I.; Lynen, F.; Van Der Voort, P. Developing a new and versatile ordered mesoporous organosilica as a pH and temperature stable chromatographic packing material. *RSC Adv.* **2015**, *5*, 5546–5552. [[CrossRef](#)]
29. Zou, H.; Wang, R.; Shi, Z.; Dai, J.; Zhang, Z.; Qiu, S. One-dimensional periodic mesoporous organosilica helical nanotubes with amphiphilic properties for the removal of contaminants from water. *J. Mater. Chem. A* **2016**, *4*, 4145–4154. [[CrossRef](#)]
30. Wei, Y.; Li, X.; Zhang, R.; Liu, Y.; Wang, W.; Ling, Y.; El-Toni, A.M.; Zhao, D. Periodic mesoporous organosilica nanocubes with ultrahigh surface areas for efficient CO₂ adsorption. *Sci. Rep.* **2016**, *6*, 20769. [[CrossRef](#)]
31. Sasidharan, M.; Nakashima, K.; Gunawardhana, N.; Yokoi, T.; Ito, M.; Inoue, M.; Yusa, S.I.; Yoshio, M.; Tatsumi, T. Periodic organosilica hollow nanospheres as anode materials for lithium ion rechargeable batteries. *Nanoscale* **2011**, *3*, 4768–4773. [[CrossRef](#)] [[PubMed](#)]
32. Li, Y.; Auras, F.; Löbermann, F.; Döblinger, M.; Schuster, J.; Peter, L.M.; Trauner, D.; Bein, T. A photoactive porphyrin-based periodic mesoporous organosilica thin film. *J. Am. Chem. Soc.* **2013**, *135*, 18513–18519. [[CrossRef](#)] [[PubMed](#)]
33. Kuroki, M.; Asefa, T.; Whitnal, W.; Kruk, M.; Yoshina-Ishii, C.; Jaroniec, M.; Ozin, G.A. Synthesis and Properties of 1,3,5-Benzene Periodic Mesoporous Organosilica (PMO): Novel Aromatic PMO with Three Point Attachments and Unique Thermal Transformations. *J. Am. Chem. Soc.* **2002**, *124*, 13886–13895. [[CrossRef](#)] [[PubMed](#)]

34. Sanchez, C.; Jeremias, F.; Ernst, S.-J.; Henninger, S.K. Synthesis, functionalization and evaluation of ethylene-bridged PMOs as adsorbents for sorption dehumidification and cooling systems. *Micropor. Mesopor. Mat.* **2017**, *244*, 151–157. [[CrossRef](#)]
35. Croissant, J.G.; Cattoën, X.; Man, M.W.C.; Gallud, A.; Raehm, L.; Trens, P.; Maynadier, M.; Durand, J.O. Biodegradable ethylene-bis(propyl)disulfide-based periodic mesoporous organosilica nanorods and nanospheres for efficient in-vitro drug delivery. *Adv. Mater.* **2014**, *26*, 6174–6180. [[CrossRef](#)]
36. Chen, Y.; Meng, Q.; Wu, M.; Wang, S.; Xu, P.; Chen, H.; Li, Y.; Zhang, L.; Wang, L.; Shi, J.L. Hollow mesoporous organosilica nanoparticles: A generic intelligent framework-hybridization approach for biomedicine. *J. Am. Chem. Soc.* **2014**, *136*, 16326–16334. [[CrossRef](#)]
37. Qian, X.; Wang, W.; Kong, W.; Chen, Y. Hollow periodic mesoporous organosilicas for highly efficient HIFU-based synergistic therapy. *RSC Adv.* **2014**, *4*, 17950–17958. [[CrossRef](#)]
38. Giret, S.; Man, M.W.C.; Carcel, C. Mesoporous-silica-functionalized nanoparticles for drug delivery. *Chem. Eur. J.* **2015**, *21*, 13850–13865. [[CrossRef](#)]
39. Wang, T.; Guan, B.; Wang, X.; Li, X.; Zhang, Y.; Qiao, Z.A.; Liu, Y.; Huo, Q. Mesostructured TiO₂ gated periodic mesoporous organosilica-based nanotablets for multistimuli-responsive drug release. *Small* **2015**, *11*, 5907–5911. [[CrossRef](#)]
40. Croissant, J.G.; Salles, D.; Maynadier, M.; Mongin, O.; Hugues, V.; Blanchard-Desce, M.; Cattoën, X.; Man, M.W.C.; Gallud, A.; Garcia, M.; et al. Mixed periodic mesoporous organosilica nanoparticles and core-shell systems, application to in vitro two-photon imaging, therapy, and drug delivery. *Chem. Mater.* **2014**, *26*, 7214–7220. [[CrossRef](#)]
41. Munaweera, I.; Hong, J.; D'Souza, A.; Balkus, K.J., Jr. Novel wrinkled periodic mesoporous organosilica nanoparticles for hydrophobic anticancer drug delivery. *J. Porous Mater.* **2014**, *22*, 1–10. [[CrossRef](#)]
42. Liu, W.; Ma, N.; Li, S.; Zhang, X.; Huo, W.-L.; Xu, J.; Meng, X.; Yang, J. A one-step method for pore expansion and enlargement of hollow cavity of hollow periodic mesoporous organosilica spheres. *J. Mater. Sci.* **2016**, *52*, 2868–2878. [[CrossRef](#)]
43. Qian, X.; Wang, W.; Kong, W.; Chen, Y. Organic-inorganic hybrid hollow mesoporous organosilica nanoparticles for efficient ultrasound-based imaging and controlled drug release. *J. Nanomater.* **2014**, *2014*, 1–8. [[CrossRef](#)]
44. Croissant, J.G.; Fatieiev, Y.; Omar, H.; Anjum, D.H.; Gurinov, A.A.; Lu, J.; Tamanoi, F.; Zink, J.I.; Khashab, N.M. Periodic mesoporous organosilica nanoparticles with controlled morphologies and high drug/dye loadings for multicargo delivery in cancer cells. *Chem. Eur. J.* **2016**, *22*, 9607–9615. [[CrossRef](#)] [[PubMed](#)]
45. Lin, C.X.; Qiao, S.; Yu, C.; Ismadji, S.; Lu, G. Periodic mesoporous silica and organosilica with controlled morphologies as carriers for drug release. *Microporous Mesoporous Mater.* **2009**, *117*, 213–219. [[CrossRef](#)]
46. Parambadath, S.; Mathew, A.; Barnabas, M.J.; Ha, C.S. A pH-responsive drug delivery system based on ethylenediamine bridged periodic mesoporous organosilica. *Micropor. Mesopor. Mater.* **2015**, *215*, 67–75. [[CrossRef](#)]
47. Jimenez, C.M.; Croissant, J.G.; Maynadier, M.; Cattoën, X.; Man, M.W.C.; Vergnaud, J.; Chaleix, V.; Sol, V.; Garcia, M.; Gary-Bobo, M.; et al. Porphyrin-functionalized mesoporous organosilica nanoparticles for two-photon imaging of cancer cells and drug delivery. *J. Mater. Chem. B* **2015**, *3*, 3681–3684. [[CrossRef](#)]
48. Lu, N.; Tian, Y.; Tian, W.; Huang, P.; Liu, Y.; Tang, Y.; Wang, C.; Wang, S.; Su, Y.; Zhang, Y.; et al. Smart cancer cell targeting imaging and drug delivery system by systematically engineering periodic mesoporous organosilica nanoparticles. *ACS Appl. Mater. Interfaces* **2016**, *8*, 2985–2993. [[CrossRef](#)]
49. Park, S.S.; Moorthy, M.S.; Ha, C.-S. Periodic mesoporous organosilica (PMO) for catalytic applications. *Korean J. Chem. Eng.* **2014**, *31*, 1707–1719. [[CrossRef](#)]
50. Sponchia, G.; Marin, R.; Freris, I.; Marchiori, M.; Moretti, E.; Storaro, L.; Canton, P.; Lausi, A.; Benedetti, A.; Riello, P. Mesoporous silica nanoparticles with tunable pore size for tailored gold nanoparticles. *J. Nanoparticle Res.* **2014**, *16*, 2245. [[CrossRef](#)]
51. Esquivel, D.; De Canck, E.; Jiménez-Sanchidrián, C.; Van Der Voort, P.; Romero-Salguero, F.J. Periodic Mesoporous organosilicas as catalysts for organic reactions. *Curr. Org. Chem.* **2014**, *18*, 1280–1295. [[CrossRef](#)]
52. Hu, H.; Liu, J.; Yu, J.; Wang, X.; Zheng, H.; Xu, Y.; Chen, M.; Han, J.; Liu, Z.; Zhang, Q. Synthesis of Janus Au@periodic mesoporous organosilica (PMO) nanostructures with precisely controllable morphology: A seed-shape defined growth mechanism. *Nanoscale* **2017**, *9*, 4826–4834. [[CrossRef](#)] [[PubMed](#)]

53. Liu, J.; Yang, H.Q.; Kleitz, F.; Chen, Z.G.; Yang, T.; Strounina, E.; Lu, G.; Qiao, S. Yolk-Shell Hybrid materials with a periodic mesoporous organosilica shell: Ideal nanoreactors for selective alcohol oxidation. *Adv. Funct. Mater.* **2011**, *22*, 591–599. [[CrossRef](#)]
54. Jacinto, M.J.; Silva, F.P.; Kiyohara, P.K.; Rossi, L.M.; Landers, R. Catalyst recovery and recycling facilitated by magnetic separation: Iridium and other metal nanoparticles. *ChemCatChem* **2012**, *4*, 698–703. [[CrossRef](#)]
55. Wang, D.; Astruc, D. Fast-growing field of magnetically recyclable nanocatalysts. *Chem. Rev.* **2014**, *114*, 6949–6985. [[CrossRef](#)]
56. Yoon, T.J.; Lee, W.; Oh, Y.S.; Lee, J.K. Magnetic nanoparticles as a catalyst vehicle for simple and easy recycling. *New J. Chem.* **2003**, *27*, 227–229. [[CrossRef](#)]
57. Mrówczyński, R.; Nan, A.; Liebscher, J. Magnetic nanoparticle-supported organocatalysts – an efficient way of recycling and reuse. *RSC Adv.* **2014**, *4*, 5927–5952. [[CrossRef](#)]
58. Polshettiwar, V.; Luque, R.; Fihri, A.; Zhu, H.; Bouhrara, M.; Basset, J.M. Magnetically recoverable nanocatalysts. *Chem. Rev.* **2011**, *111*, 3036–3075. [[CrossRef](#)]
59. Lim, C.W.; Lee, I.S. Magnetically recyclable nanocatalyst systems for the organic reactions. *Nano Today* **2010**, *5*, 412–434. [[CrossRef](#)]
60. Zhang, N.; Zhou, C.; Sun, Z.; Wu, L.Z.; Tung, C.; Zhang, T. Magnetically recyclable nanocatalysts (MRNCs): A versatile integration of high catalytic activity and facile recovery. *Nanoscale* **2012**, *4*, 6244–6255. [[CrossRef](#)]
61. Baig, R.B.N.; Varma, R.S. Magnetically retrievable catalysts for organic synthesis. *Chem. Commun.* **2013**, *49*, 752–770. [[CrossRef](#)] [[PubMed](#)]
62. Shylesh, S.; Schünemann, V.; Thiel, W.R. Magnetically separable nanocatalysts: Bridges between homogeneous and heterogeneous catalysis. *Angew. Chem. Int. Ed.* **2010**, *49*, 3428–3459. [[CrossRef](#)] [[PubMed](#)]
63. Kalidindi, S.B.; Jagirdar, B.R. Nanocatalysis and prospects of green chemistry. *ChemSusChem* **2011**, *5*, 65–75. [[CrossRef](#)] [[PubMed](#)]
64. Gawande, M.B.; Branco, P.S.; Varma, R.S. Nano-magnetite (Fe₃O₄) as a support for recyclable catalysts in the development of sustainable methodologies. *Chem. Soc. Rev.* **2013**, *42*, 3371–3393. [[CrossRef](#)] [[PubMed](#)]
65. Karimi, B.; Mansouri, F.; Mirzaei, H.M. ChemInform abstract: Recent applications of magnetically recoverable nanocatalysts in C-C and C-X coupling reactions. *ChemCatChem* **2015**, *46*, 1736–1789. [[CrossRef](#)]
66. Kudr, J.; Haddad, Y.; Richtera, L.; Heger, Z.; Cernak, M.; Adam, V.; Zitka, O. Magnetic nanoparticles: From design and synthesis to real world applications. *Nanomaterials* **2017**, *7*, 243. [[CrossRef](#)]
67. Akbarzadeh, A.; Samiei, M.; Davaran, S. Magnetic nanoparticles: Preparation, physical properties, and applications in biomedicine. *Nanoscale Res. Lett.* **2012**, *7*, 1–14. [[CrossRef](#)]
68. Lu, A.H.; Salabas, E.L.; Schuth, F. Magnetic nanoparticles: Synthesis, protection, functionalization, and application. *Angew. Chem. Int. Ed.* **2007**, *46*, 1222–1244. [[CrossRef](#)]
69. Faraji, M.; Yamini, Y.; Rezaee, M. Magnetic nanoparticles: Synthesis, stabilization, functionalization, characterization, and applications. *J. Iran. Chem. Soc.* **2010**, *7*, 1–37. [[CrossRef](#)]
70. Yiu, H.H.P.; Keane, M.A. Enzyme-magnetic nanoparticle hybrids: New effective catalysts for the production of high value chemicals. *J. Chem. Technol. Biotechnol.* **2012**, *87*, 583–594. [[CrossRef](#)]
71. Khoshnevisan, K.; Vakhshiteh, F.; Barkhi, M.; Baharifar, H.; Poor-Akbar, E.; Zari, N.; Stamatis, H.; Bordbar, A.K. Immobilization of cellulase enzyme onto magnetic nanoparticles: Applications and recent advances. *Mol. Catal.* **2017**, *442*, 66–73. [[CrossRef](#)]
72. Cristea, C.; Tertis, M.; Galatus, R.V. Magnetic nanoparticles for antibiotics detection. *Nanomaterials* **2017**, *7*, 119. [[CrossRef](#)] [[PubMed](#)]
73. Gijs, M.A.M.; Lacharme, F.; Lehmann, U. Microfluidic applications of magnetic particles for biological analysis and catalysis. *Chem. Rev.* **2010**, *110*, 1518–1563. [[CrossRef](#)] [[PubMed](#)]
74. Ha, Y.; Ko, S.; Kim, I.; Huang, Y.; Mohanty, K.K.; Huh, C.; Maynard, J.A. Recent advances incorporating superparamagnetic nanoparticles into immunoassays. *ACS Appl. Nano Mater.* **2018**, *1*, 512–521. [[CrossRef](#)]
75. Wang, D.; He, J.; Rosenzweig, N.; Rosenzweig, Z. Superparamagnetic Fe₂O₃Beads–CdSe/ZnS quantum dots core–shell nanocomposite particles for cell separation. *Nano Lett.* **2004**, *4*, 409–413. [[CrossRef](#)]
76. Fallah-Mehrjardi, M. Fe₃O₄@silica sulfuric acid: An efficient and heterogeneous nanomagnetic catalyst in organic reactions. *Mini-Rev. Org. Chem.* **2017**, *14*, 122–129. [[CrossRef](#)]
77. Zhu, Y.; Stubbs, L.P.; Ho, F.; Liu, R.; Ship, C.P.; Maguire, J.A.; Hosmane, N.S. Magnetic nanocomposites: A new perspective in catalysis. *ChemCatChem* **2010**, *2*, 365–374. [[CrossRef](#)]

78. Rossi, L.M.; Costa, N.J.S.; Silva, F.P.; Wojcieszak, R. Magnetic nanomaterials in catalysis: Advanced catalysts for magnetic separation and beyond. *Green Chem.* **2014**, *16*, 2906–2933. [[CrossRef](#)]
79. Dong, C.D.; Chen, C.W.; Chang, S.H. Magnetic nanoparticles and their heterogeneous persulfate oxidation organic compound applications. *Springer Proc. Phys.* **2015**, *175*, 23–35. [[CrossRef](#)]
80. Larsen, G.K.; Farr, W.; Hunyadi Murph, S.E. Multifunctional Fe₂O₃-Au nanoparticles with different shapes: Enhanced catalysis, photothermal effects, and magnetic recyclability. *J. Phys. Chem. C* **2016**, *120*, 15162–15172. [[CrossRef](#)]
81. Schätz, A.; Reiser, O.; Stark, W.J. Nanoparticles as semi-heterogeneous catalyst supports. *Chem. Eur. J.* **2010**, *16*, 8950–8967. [[CrossRef](#)] [[PubMed](#)]
82. Fan, J.; Gao, Y. Nanoparticle-supported catalysts and catalytic reactions—A mini-review. *J. Exp. Nanosci.* **2006**, *1*, 457–475. [[CrossRef](#)]
83. Mulahmetovic, E.; Hargaden, G.C. Recent advances in the development of magnetic catalysts for the Suzuki reaction. *Rev. J. Chem.* **2017**, *7*, 373–398. [[CrossRef](#)]
84. Rossi, L.M.; Garcia, M.A.S.; Vono, L.L.R. Recent advances in the development of magnetically recoverable metal nanoparticle catalysts. *J. Braz. Chem. Soc.* **2012**, *23*, 1959–1971. [[CrossRef](#)]
85. Cardoso, V.F.; Francesko, A.; Ribeiro, C.; Bañobre-Lopez, M.; Martins, P.; Lanceros-Méndez, S. Advances in magnetic nanoparticles for biomedical applications. *Adv. Health Mater.* **2017**, *7*, 1700845. [[CrossRef](#)]
86. Pankhurst, Q.A.; Connolly, J.; Jones, S.K.; Dobson, J. Applications of magnetic nanoparticles in biomedicine. *J. Phys. D Appl. Phys.* **2003**, *36*, R167–R181. [[CrossRef](#)]
87. Xu, C.; Xu, K.; Gu, H.; Zheng, R.; Liu, H.; Zhang, X.; Guo, Z.; Xu, B. Dopamine as a robust anchor to immobilize functional molecules on the iron oxide shell of magnetic nanoparticles. *J. Am. Chem. Soc.* **2004**, *126*, 9938–9939. [[CrossRef](#)]
88. Vedernikova, I.A. Magnetic nanoparticles: Advantages of using, methods for preparation, characterization, application in pharmacy. *Rev. J. Chem.* **2015**, *5*, 256–280. [[CrossRef](#)]
89. Zverev, V.; Pyatakov, A.; Shtil, A.; Tishin, A. Novel applications of magnetic materials and technologies for medicine. *J. Magn. Magn. Mater.* **2018**, *459*, 182–186. [[CrossRef](#)]
90. Neuberger, T.; Schöpf, B.; Hofmann, H.; Hofmann, M.; Von Rechenberg, B. Superparamagnetic nanoparticles for biomedical applications: Possibilities and limitations of a new drug delivery system. *J. Magn. Magn. Mater.* **2005**, *293*, 483–496. [[CrossRef](#)]
91. Mosayebi, J.; Kiyasatfar, M.; Laurent, S. Synthesis, functionalization, and design of magnetic nanoparticles for theranostic applications. *Adv. Health Mater.* **2017**, *6*, 1700306. [[CrossRef](#)] [[PubMed](#)]
92. Zhang, L.; Qiao, S.; Jin, Y.G.; Chen, Z.G.; Gu, H.C.; Lu, G. Magnetic hollow spheres of periodic mesoporous organosilica and Fe₃O₄ nanocrystals: Fabrication and structure control. *Adv. Mater.* **2008**, *20*, 805–809. [[CrossRef](#)]
93. Li, J.; Wei, Y.; Li, W.; Deng, Y.; Zhao, D. Magnetic spherical cores partly coated with periodic mesoporous organosilica single crystals. *Nanoscale* **2012**, *4*, 1647–1651. [[CrossRef](#)] [[PubMed](#)]
94. Yang, Y.; Zhang, W.; Yang, F.; Zhou, B.; Zeng, D.; Zhang, N.; Zhao, G.; Hao, S.; Zhang, X. Ru nanoparticles dispersed on magnetic yolk-shell nanoarchitectures with Fe₃O₄ core and sulfoacid-containing periodic mesoporous organosilica shell as bifunctional catalysts for direct conversion of cellulose to isosorbide. *Nanoscale* **2018**, *10*, 2199–2206. [[CrossRef](#)] [[PubMed](#)]
95. Lin, C.X.; Li, Z.; Brumbley, S.; Petrasovits, L.; McQualter, R.B.; Yu, C.; Lu, G. Synthesis of magnetic hollow periodic mesoporous organosilica with enhanced cellulose tissue penetration behaviour. *J. Mater. Chem.* **2011**, *21*, 7565–7571. [[CrossRef](#)]
96. Lan, F.; Hu, H.; Jiang, W.; Liu, K.; Zeng, X.; Wu, Y.; Gu, Z. Synthesis of superparamagnetic Fe₃O₄/PMMA/SiO₂ nanorattles with periodic mesoporous shell for lysozyme adsorption. *Nanoscale* **2012**, *4*, 2264–2267. [[CrossRef](#)]
97. Wei, Y.; Li, X.; Elzatahry, A.; Zhang, R.; Wang, W.; Tang, X.; Yang, J.; Wang, J.; Al-Dahyan, D.; Zhao, D. A versatile in situ etching-growth strategy for synthesis of yolk-shell structured periodic mesoporous organosilica nanocomposites. *RSC Adv.* **2016**, *6*, 51470–51479. [[CrossRef](#)]
98. Stöber, W.; Fink, A.; Bohn, E. Controlled growth of monodisperse silica spheres in the micron size range. *J. Colloid Interface Sci.* **1968**, *26*, 62–69. [[CrossRef](#)]
99. Ma, Z.Y.; Liu, X.Q.; Guan, Y.P.; Liu, H.Z. Synthesis of magnetic silica nanospheres with metal ligands and application in affinity separation of proteins. *Colloids Surfaces A Physicochem. Eng. Asp.* **2006**, *275*, 87–91. [[CrossRef](#)]

100. Lu, Y.; Yin, Y.; Mayers, B.T.; Xia, Y. Modifying the surface properties of superparamagnetic iron oxide nanoparticles through a sol–gel approach. *Nano Lett.* **2002**, *2*, 183–186. [[CrossRef](#)]
101. Santra, S.; Tapeç, R.; Theodoropoulou, N.; Dobson, J.; Hebard, A.; Tan, W. Synthesis and characterization of silica-coated iron oxide nanoparticles in microemulsion: The effect of nonionic surfactants. *Langmuir* **2001**, *17*, 2900–2906. [[CrossRef](#)]
102. Massart, R. Preparation of aqueous magnetic liquids in alkaline and acidic media. *IEEE Trans. Magn.* **1981**, *17*, 1247–1248. [[CrossRef](#)]
103. Axet, M.; Philippot, K. Catalysis with colloidal ruthenium nanoparticles. *Chem. Rev.* **2020**, *120*, 1085–1145. [[CrossRef](#)] [[PubMed](#)]
104. Rakers, L.; Martínez-Prieto, L.M.; López-Vinasco, A.M.; Philippot, K.; Chaudret, B.; Glorius, F.; Van Leeuwen, P.W.N.M. Ruthenium nanoparticles ligated by cholesterol-derived NHCs and their application in the hydrogenation of arenes. *Chem. Commun.* **2018**, *54*, 7070–7073. [[CrossRef](#)]
105. Novio, F.; Monahan, D.; Coppel, Y.; Antorrena, G.; Lecante, P.; Philippot, K.; Chaudret, B. Surface chemistry on small ruthenium nanoparticles: Evidence for site selective reactions and influence of ligands. *Chem. Eur. J.* **2014**, *20*, 1287–1297. [[CrossRef](#)]
106. Rafter, E.; Gutmann, T.; Löw, F.; Buntkowsky, G.; Philippot, K.; Chaudret, B.; Van Leeuwen, P.W.N.M. Secondary phosphineoxides as pre-ligands for nanoparticle stabilization. *Catal. Sci. Technol.* **2013**, *3*, 595–599. [[CrossRef](#)]
107. Lara, P.; Philippot, K.; Chaudret, B. ChemInform abstract: Organometallic ruthenium nanoparticles: A comparative study of the influence of the stabilizer on their characteristics and reactivity. *ChemCatChem* **2013**, *44*, 28–45. [[CrossRef](#)]
108. González-Gálvez, D.; Nolis, P.; Philippot, K.; Chaudret, B.; Van Leeuwen, P.W.N.M. Phosphine-stabilized ruthenium nanoparticles: The effect of the nature of the ligand in catalysis. *ACS Catal.* **2012**, *2*, 317–321. [[CrossRef](#)]



© 2020 by the authors. Licensee MDPI, Basel, Switzerland. This article is an open access article distributed under the terms and conditions of the Creative Commons Attribution (CC BY) license (<http://creativecommons.org/licenses/by/4.0/>).